Biochimica et Biophysica Acta 1822 (2012) 1137–1146

Contents lists available at SciVerse ScienceDirect

Biochimica et Biophysica Acta

journal homepage: www.elsevier.com/locate/bbadis

Lysosomal di-N-acetylchitobiase-deficient mouse tissues accumulate Man2GlcNAc2 and Man3GlcNAc2

Emanuele Persichetti [a], Katharina Klein [b], Silvia Paciotti [a], Karine Lecointe [c], Chiara Balducci [a], Sebastian Franken [b], Sandrine Duvet [c], Ulrich Matzner [b], Rita Roberti [d], Dieter Hartmann [e], Volkmar Gieselmann [b], Tommaso Beccari [a,*]

[a] University of Perugia, D.S.E.E.A., Institute of Food Chemistry, Biochemistry, Physiology and Nutrition, 06126 Perugia, Italy
[b] Institut für Biochemie und Molekularbiologie, Nussallee 11, Rheinische Friedrich-Wilhelms-Universität Bonn, 53115 Bonn, Germany
[c] Unité de Glycobiologie Structurale et Fonctionnelle,UMR/CNRS 8576,IFR147, Université des Sciences et Technologies de Lille,F-59655 Villeneuve d'Ascq, France
[d] University of Perugia, Department of Internal Medicine, Laboratory of Biochemistry, via del Giochetto, 06122 Perugia, Italy
[e] Institute of Anatomy, Division of Neuroanatomy, University of Bonn, Nussallee 10, 53115 Bonn, Germany

ARTICLE INFO

Article history:
Received 2 December 2011
Received in revised form 1 March 2012
Accepted 12 March 2012
Available online 20 March 2012

Keywords:
Lysosomal di-N-acetylchitobiase
Lysosomal storage disease
Knockout mouse
N-linked glycan

ABSTRACT

Most lysosomal storage diseases are caused by defects in genes encoding for acidic hydrolases. Deficiency of an enzyme involved in the catabolic pathway of N-linked glycans leads to the accumulation of the respective substrate and consequently to the onset of a specific storage disorder. Di-N-acetylchitobiase and core specific α1–6mannosidase represent the only exception. In fact, to date no lysosomal disease has been correlated to the deficiency of these enzymes. We generated di-N-acetylchitobiase-deficient mice by gene targeting of the Ctbs gene in murine embryonic stem cells. Accumulation of Man2GlcNAc2 and Man3GlcNAc2 was evaluated in all analyzed tissues and the tetrasaccharide was detected in urines. Multilamellar inclusion bodies reminiscent of polar lipids were present in epithelia of a scattered subset of proximal tubules in the kidney. Less constantly, enlarged Kupffer cells were observed in liver, filled with phagocytic material resembling partly digested red blood cells. These findings confirm an important role for lysosomal di-N-acetylchitobiase in glycans degradation and suggest that its deficiency could be the cause of a not yet described lysosomal storage disease.

1. Introduction

During the degradation of glycoproteins with asparagine-linked carbohydrates, the N-acetylglucosamine residue at the reducing end of the N,N′ diacetylchitobiose core of oligosaccharides is hydrolyzed by the lysosomal glycosidase di-N-acetylchitobiase (chitobiase) (EC 3.2.1.-) [1]. This enzyme was first purified and characterized in human liver [2]; human and rat chitobiase cDNAs were cloned [3].

To date, no storage disease has been described in humans or animals as a result of chitobiase deficiency. However, cloning and characterization of the human core-specific lysosomal α1–6mannosidase (MAN2B2) demonstrated that this enzyme is dependent on chitobiase activity [4–7] during the degradation of the Manα1–3[Manα1–6]Manβ1–4GlcNAcβ1–4GlcNAc core structure resulting from the catabolism of N-linked oligosaccharides (Fig. 1, panel A). While lysosomal α-mannosidase (LysMan) can cleave the Manα1–3 from the non-reducing end of this structure, the efficient removal of Manα1–6 residue by α1–6mannosidase requires the trimming of the reducing terminal GlcNAc by chitobiase. These data are confirmed by the accumulation of Manα1–6Manβ1–4GlcNAcβ1–4GlcNAc-Asn in tissues of N-aspartylglucosaminidase-deficient mice [8], a mouse model for the lysosomal disorder aspartylglycosaminuria.

Chitobiase, as well as lysosomal α1–6mannosidase, is expressed only in humans and rodents, whereas alterations in promoter sequence inhibit its expression in ruminants, felines and dogs [9,10]. This difference could explain the variation in the glycan structures accumulated in subjects affected by alpha-mannosidosis, a lysosomal storage disease caused by the genetic deficiency of α-mannosidase, in various species. In cattle, cats and dogs a deficiency of α-mannosidase causes the accumulation of the tri-mannosyl core (Manα1–3[Manα1–6]Manβ1–4-GlcNAcβ1–4GlcNAc) in addition to the extended structures on the α1–3Man branch [11]. In humans and rodents the main stored structure is Manα1–3Manβ1–4GlcNAc, along with other extended products on the α1–3Man branch [6,12,13].

The murine gene encoding the chitobiase (Ctbs) has been recently cloned [14]. The gene spans about 15 kb from the transcription initiation site to the translation stop codon and includes 7 exons, like

* Corresponding author at: Università di Perugia, D.S.E.E.A., Via San Costanzo, 06121 Perugia, Italy. Tel.: +39 075 5857441; fax: +39 075 5857904.
E-mail address: tbeccari@unipg.it (T. Beccari).

0925-4439/$ – see front matter © 2012 Elsevier B.V. All rights reserved.
doi:10.1016/j.bbadis.2012.03.005

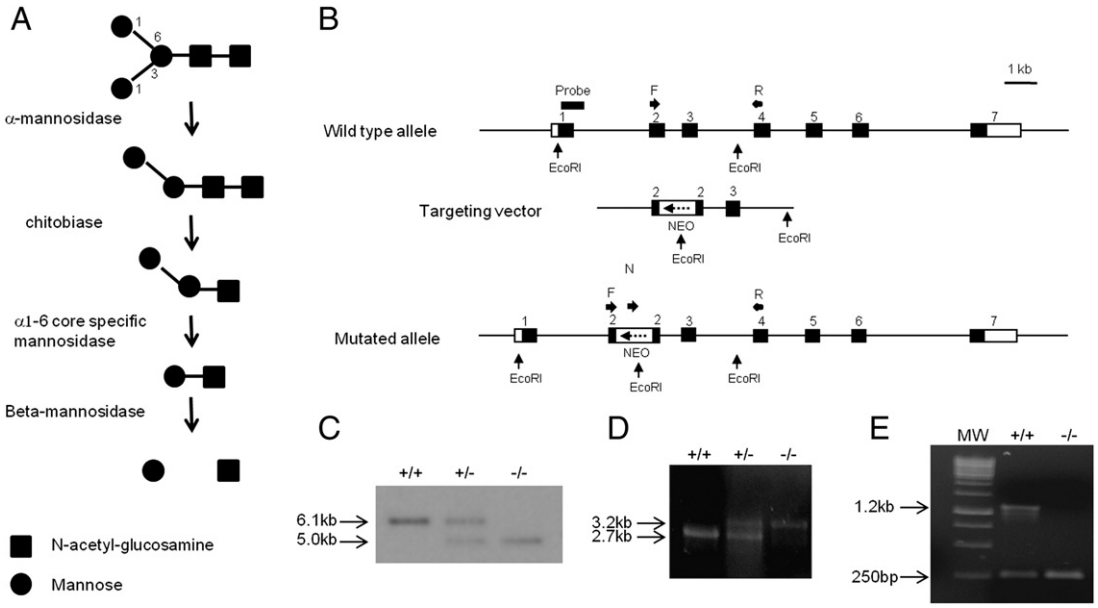

Fig. 1. Degradation of the N-linked glycan core and targeted disruption of Ctbs gene. (A) Stepwise trimming of the glycan core derived from N-linked oligosaccharides. The removal of the terminal N-acetyl-glucosamine by chitobiase is essential for the core specific α1–6 mannosidase activity. (B) Schematic representation of the endogenous Ctbs gene, the targeting construct and the disrupted allele. Boxes are the exons. Black parts indicate coding regions, white parts represent non-coding regions. The 5′ probe used for Southern blot is indicated, as well as primers used to screen recombinant ES clones and mouse litters (F, R, N). Arrow within the NEO cassette indicates transcriptional orientation. (C) Southern blot analysis of liver genomic DNA. EcoRI digested DNA of wild type (+/+), heterozygous (+/−) and KO (−/−) mice was separated on an agarose gel, blotted and hybridized with the 5' probe. The 6.1 kb band corresponds to the wild type allele, the 5.0 kb band represents the mutant allele. (D) PCR genotyping of mouse tail DNA. Primers F, R and N were used in the same reaction. 3.2 kb and 2.7 kb bands correspond to mutated and wild type allele, respectively. (E) RT-PCR of kidney RNA. RNA of wild type and CTBS deficient mice was retrotranscribed and PCR amplified. 1.2 kb band represents the main CTBS transcript, obtained with a primer forward on 5′ UTR and a primer reverse on 3′ UTR. 250 bp band corresponds to a fragment of beta-actin cDNA, used as an internal control.

the human CTBS gene [10]. The amino acid sequences of murine and human enzymes show 79% identity and 86% similarity.

In this study, we present the first chitobiase-deficient mouse model. In order to disrupt the Ctbs gene, the open reading frame of the neomycin resistance gene (NEO) was inserted in exon 2. RT PCR, enzyme assay and Western blotting analyses confirmed that no detectable amount of chitobiase was expressed in chitobiase KO mice. Although no overt phenotypical alteration is evident, significant amounts of the Man2GlcNAc2 tetrasaccharide and, to a minor extent, of the Man3GlcNAc2 pentasaccharide accumulate in several KO tissues. Histological analysis reveals typical features of other murine models of lysosomal storage diseases: firstly and more evidently the presence of multilamellar inclusion bodies indicative of polar lipids in epithelial cells of scattered proximal kidney tubules, in addition to enlarged vacuolated Kupffer cells. Preliminary data from lectin screening indicate that mannosyl compounds may accumulate even in those epithelial cells that are still devoid of ultrastructurally visible storage material.

The accumulation of oligosaccharides and the pathological features observed in this mouse model provide the first *in vivo* evidence of the crucial role of chitobiase in glycans degradation. Since the role of chitobiase is the same in mice and humans, this result suggests that the genetic lack of chitobiase could be the cause of a not yet described human lysosomal storage disease.

2. Materials and methods

2.1. Construction of the targeting vector

A 5.4 kb XbaI fragment obtained from the Mouse Genomic λ FIX II library (Stratagene) and corresponding to the region from intron 1 to intron 3 of mouse ctbs gene was cloned in pBlueScript SK (Stratagene). A BamHI site was created into exon 2 by site directed mutagenesis. This site was used to subclone the NEO gene from pBSK-NEO vector. Orientation of this fragment was confirmed by restriction analysis. The entire cassette was sequenced.

2.2. Generation of chitobiase knockout mice

200 micrograms of the targeting vector were linearized with NotI and introduced into 3×107 HM-1 murine embryonic stem (ES) cells [15] by electroporation (Bio-Rad Gene Pulser II; 0.8 kV, 3 μF). The ES cells were maintained on feeder layers under the selective pressure of G418 containing medium (Sigma-Aldrich) for 8 days. ES cell clones were picked, expanded and screened by PCR for homologous recombination. Targeted clones were reconfirmed by Southern blot analysis after digestion with EcoRI and hybridization with a 5' external probe. ES cells from two targeted clones were microinjected into blastocysts from C57BL/6 N (Charles River) mice and transferred to pseudopregnant recipient females. A total of 10 chimerae were born, with a high contribution of agouti coat colour. The chimeric animals were bred with C57BL/6 N mice, and agouti pups were screened for germ line transmission of the mutant allele. The genotypes of the offspring of these matings and all subsequent offspring were determined by PCR on DNA from tail biopsy specimens.

The following primers were used: ctbsFOR (primer F in Fig. 1), 5′-ATGACTGGTCACAGATTACAACTG-3′; ctbsREV (primer R), 5′-ATGGTG ATCAACAAGGATGAGTATC-3′; NEOREV (primer N), 5′-ACTTCGCCCA ATAGCAGCCAG-3′. PCR conditions were the following: denaturation 98 °C for 3 min, followed by 35 cycles of 30 sec at 98 °C, 30 sec at 64 °C and 90 sec at 72 °C. The PCR resulted in fragments of 2700 bp for the wild-type and 3200 bp for the mutant fragment.

Mice used in this study were housed under standard conditions in a 12-h light–dark cycle with food and water ad libitum. All experiments were carried out in accordance with local and state regulations for research with animals.

2.3. Gel filtration chromatography

Liver and kidney of WT and KO mice were homogenized in 50 mM phosphate buffer pH 7.0 containing 150 mM sodium chloride (1:5, w/v) and centrifuged at 15,000 ×*g* for 20 min. The supernatant was centrifuged a second time at the same conditions and passed through a syringe packed with glass wool. The flowthrough was centrifuged at 15,000 ×*g* for 10 min. All centrifugation steps were performed at 4 °C. The final supernatant was applied to a 1.5×66-cm ACA-44 (LKB) gel filtration column equilibrated with 50 mM phosphate buffer (pH 7.0) containing 150 mM sodium chloride and resolved at a flow rate of 0.66 ml/min. 1 ml fractions were collected for determination of β-hexosaminidase (β-Hex) and chitobiase activity.

2.4. β-Hexosaminidase, α-mannosidase, β-glucosidase and chitobiase assay

β-Hexosaminidase and α-mannosidase activity was measured using 3 mM 4-Methylumbelliferyl N-acetyl-β-D-glucosaminide (MUG) (Toronto Research Chemicals) and 3 mM 4-Methylumbelliferyl α-D-mannopyranoside (Sigma-Aldrich), respectively, in 0.1 M citric acid/0.2 M disodium phosphate buffer (pH 4.5). β-glucosidase was measured using 3 mM 4-Methylumbelliferyl β-D-glucopyranoside (Sigma-Aldrich) in 0.1 M citric acid/0.2 M disodium phosphate buffer (pH 5.0) with 0.2% taurodeoxycholic acid. The fluorescence of the liberated 4-methylumbelliferone was measured using a PerkinElmer LS B50 fluorimeter ($\lambda_{excitation}=360$ nm; $\lambda_{emission}=446$ nm). One unit is the amount of enzyme that hydrolyses 1 μmol of substrate in 1 min at 37 °C.

Chitobiase activity was determined incubating 33 μl sample with 34 μl 10 mM chitobiose (Toronto Research Chemicals) in 0,1 M citrate /0.2 M disodium phosphate buffer (pH 3.5). After an appropriate incubation time at 37 °C, 33 μl 0.8 M potassium tetraborate pH 10.4 were added, the sample was heated 3 min at 100 °C and cooled in ice. 1 ml p-dimethylaminobenzaldehyde (DMAB) (prepared by dissolving 10 g DMAB in 100 ml glacial acetic acid containing 12.5% (v/v) 10 N HCl and diluting this reagent 1:10 in acetic acid shortly before use) were added and the reaction was conducted for 10 min at 37 °C. Samples were cooled in ice and the amount of liberated N-acetylglucosamine was determined using a spectrophotometer ($\lambda_{Abs}=585$ nm). One unit is the amount of enzyme that hydrolyses 1 μmol of substrate in 1 min at 37 °C.

2.5. Real time PCR

Real time PCR was used to quantify mRNA for β-Hex, α-mannosidase and β-glucosidase genes expressed by WT and KO 40-week-old mice tissues using eukaryotic 18S rRNA as an endogenous control gene. Pre-designed TaqMan® Gene expression assays were purchased by Applied Biosystems (primer probe set IDs: β-Hex Mm01282432_m1; α-mannosidase Mm00487585_m1; β-glucosidase Mm00484700_m1; 18S Hs99999901_s1) and a 7300 Real-Time PCR System (Applied Biosystems) was used according to the manufacturer's instructions. Threshold cycle (Ct) data for target and control genes were used to calculate ΔCt values [ΔCt = Ct (target gene) − Ct (18 s RNA)]. Then, ΔΔCt values were calculated [ΔΔCt = ΔCt (KO tissue) − ΔCt (WT tissue)]. The expression fold change was calculated as $2^{-\Delta\Delta Ct}$.

2.6. Production of an anti-CTBS polyclonal antibody

A GST-Ctbs fusion protein was obtained by cloning a 201 bp fragment, corresponding to bases from 327 to 528 of murine Ctbs cDNA, into pGEX-4T-1 plasmid (Amersham Biosciences). BL21 *E. coli* cells were transformed with this pGEX-Ctbs plasmid and the recombinant protein was purified by using Glutathione Sepharose 4B (Amersham Biosciences), following the manufacturer's protocol. Two New Zealand white rabbits (Charles River) were immunized with the purified GST-CTBS protein to raise the anti-CTBS polyclonal antibody. The rabbits were injected with a mixture of 500 μg of purified protein mixed with an equal volume of complete Freund's adjuvant. The immunization was repeated twice with 200 μg protein, after 2 weeks from the precedent injection. 10 days after the final injection, antiserum was harvested from the carotid artery and stored at −80 °C. Antibody was purified by dilution in blocking buffer (TBS with 0.1%Tween, 5% non fat milk) and O/N incubation on a nitrocellulose strip where GST-Ctbs had been blotted. After 3 washes in TBS-Tween, antibody was eluted in 100 mM glycine buffer, pH 3.5. pH was immediately neutralized with 0.2 M Na_2HPO_4.

2.7. Histology

Mice were killed by an overdose of anaesthetics and fixed by sequential transcardiac perfusion with phosphate buffer w/ 1% procaine followed by either 6% glutaraldehyde or a modified Bouin's solution, the latter corresponding to the standard Bouin mixture diluted 1:3 in Dulbecco PBS.

(Tissues were fixed o/n in the same solutions and in the case of Bouin fixation stored in 1% neutral buffered formaline.)

For immunohistochemistry and lectin histochemistry, tissues from modified Bouin-fixed mice were either embedded in low-melting-point paraffine wax and sectioned at 7 μm or (to avoid extraction by organic solvents during embedding) were directly cut on a vibratome at 20 μm.

For transmission electron microscopy, glutaraldehyde-fixed tissues were postfixed in 2% osmium tetroxide, dehydrated and embedded in Spurr's medium after passage through propylene oxide as an intermediate. Blocks were semithin sectioned at 1 μm for high resolution light microscopy after staining with either toluidine blue/pyronine G or the lipid-selective p-phenylenediamine, trimmed to regions of interest and were then recut at 70 nm for TEM, TEM sections were contrasted with lead citrate/uranyl acetate prior to evaluation. Light microscopy images were recorded on a Nikon 90i photomicroscope.

2.8. Lipid analysis of kidney

Lipids were extracted from kidneys and analyzed as previously described [16]. An aliquot of the total lipid extract was hydrolyzed under alkaline conditions to remove phospholipids. This was done to allow the quantification of sphingolipids. To detect a possible accumulation of phospholipids or sphingolipids total lipids and alkali-stable lipids, respectively, were analyzed separately on the same plate by TLC using reference standards. Separated lipids were visualized according to Yao and Rastetter [17] and quantified by densitometry scanning [16].

2.9. Extraction of soluble oligosaccharides

A sample of the various tissues originating from WT and chitobiase KO mice were homogenized in an ice-cold KMH buffer (110 mM potassium acetate, 2 mM magnesium acetate, 20 mM Hepes, pH 7.2) containing a protease inhibitor cocktail (complete, Roche Diagnostics) by using a Potter–Elvehjem homogenizer (750 rpm; five strokes). The cellular homogenate was then submitted to lipid extraction by addition of 3 ml of $CHCl_3$/MeOH/H_2O (3/2/1, v/v/v) (Kmiecik et al., 1995) [18]. The aqueous phase resulting from the lipid extraction was then lyophilized.

2.10. α-mannosidase digestions

Alpha-mannosidase digestions were carried out using the following conditions : jack bean α-mannosidase (EC 3.2.1.24, Sigma Aldrich), 0.5 U of enzyme in 200 μl 50 mM ammonium acetate buffer pH 4.5; α1,2 mannosidase (EC 3.2.1.113, isolated from *Aspergillus saitoi*,

Glyko, UK), 0.5 U of enzyme in 200 µl 20 mM sodium acetate buffer pH 5. Enzyme digestions were incubated at 37 °C for 48 h with a fresh aliquot of enzyme added after 24 h and terminated by boiling for 10 min before lyophilization. Samples were then permethylated for MALDI-MS and GC-MS analysis.

2.11. Permethylation of free oligosaccharides and disaccharide standard

Permethylation of the freeze-dried oligosaccharides and sample clean-up were performed as described [19]. Internal standards (Galβ1,4GlcNAc)and (Fuc α1,2 Galβ1,4GlcNAc)were permethylated under the same conditions.

2.12. MALDI TOF-MS analysis

For each tissue sample, permethylated oligosaccharides were mixed with a known amount of permethylated standard disaccharide (Galβ1,4 GlcNAc). For urine samples, the standard was the permethylated Fuc α1,2 Galβ1,4GlcNAc). Total permethylated oligosaccharides were cocrystallized with 2,5-dihydroxybenzoic acid as matrix (10 mg/ml 2,5-dihydroxybenzoic acid in methanol/water solution (50/50)) and freeze-dried.

MALDI-TOF-MS experiments were carried out on a Voyager Elite DE-STR Pro instrument (PerSeptive Biosystems, Framingham, MA) equipped with a pulsed nitrogen laser (337 nm) and a gridless delayed extraction ion source. The spectrometer was operated in the positive reflectron mode by delayed extraction with an accelerating voltage of 20 kV, a pulse delay time of 250 ns, and a grid voltage of 72%. All spectra represent accumulated spectra obtained by 500 laser shots. For each condition, three samples were spotted and the amount of each oligosaccharide was relatively quantified and estimated by calculating the ratio between the relative amount of these oligosaccharides and the internal standard in the MALDI-MS spectra. Protein concentration of each tissue sample was measured by a micro BCA Protein assay reagent kit (Pierce).

2.13. Linkage analysis and GC/MS analysis

The permethylated free oligosaccharides were hydrolyzed in 300 µl of 4 M TFA at 100 °C for 4 h. After removing TFA by drying *in vacuo*, the permethylated compounds were then reduced at room temperature overnight by adding 300 µl of 2 M ammonia solution containing sodium borodeuteride (10 mg/ml). The reduction was terminated by adding acetic acid, and borates were eliminated under a stream of nitrogen in the presence of methanol containing 5% (v/v) acetic acid. After adding 50 µl of pyridine and 200 µl of acetic anhydride, peracetylation was carried out at 100 °C for 2 h. After evaporation under a stream of nitrogen, the partially methylated alditol acetates (PMAAs) were dissolved in chloroform, and the chloroform phase was washed 7 times with water. This PMAA-containing phase was finally dried under a stream of nitrogen, and the PMAAs were dissolved in acetonitrile before GC-MS analysis. GC separation of PMAAs was performed using a Carbo Erba GC 8000 gas chromatograph fitted with a 25-m–0.32-mm CP-Sil5 CB low bleed capillary column, 0.25-m film phase (Chrompack France, Les Ullis, France). The temperature of the Ross injector was 260 °C. Samples were analyzed using a temperature program starting by a gradient of 2 °C/ min from 130 to 180 °C after 2 min at 130 °C followed by a gradient of 4 °C/min until 240 °C. The column was coupled to a Finnigan Automass II mass spectrometer. PMAA analyses were performed in the electron impact mode using an ionization energy of 70 eV. Relative abundance of the various PMAA derivatives was carried out using total ion current of the MS detector in the positive ion mode.

3. Results

3.1. Generation of Ctbs-deficient mice

We generated a null allele of the Ctbs gene by homologous recombination in embryonic stem (ES) cells. The targeting construct inserted the coding sequence of the neomycin resistance gene (NEO) in exon 2 of the Ctbs gene (Fig. 1, panel B).

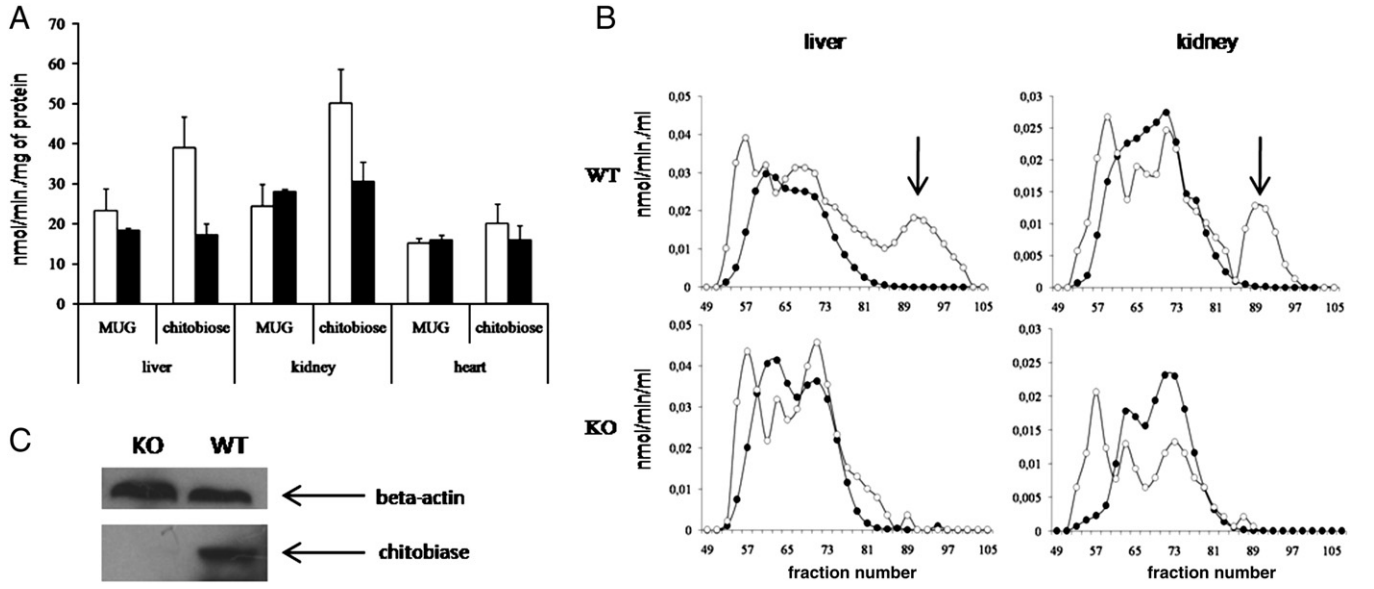

Fig. 2. Evidence of chitobiase deficiency. (A) Specific activity in 10-week-old wild type (white bars) and Ctbs-deficient (black bars) liver, kidney and heart towards two substrates, MUG and chitobiose. Chitobiase is expressed at high levels in liver and kidney, while heart is representative of tissues where chitobiase is expressed at low levels. Error bars represent one standard deviation of three WT and three KO tissues. (B) Gel filtration of wild type (WT) and chitobiase-deficient (KO) liver and kidney. Tissue extracts were applied to a 1.5×66-cm ACA-44 LKB gel filtration column. MUG (filled circles) and chitobiose (empty circles) were used as substrates. Arrows indicate the peak corresponding to chitobiase activity, absent in KO tissues. (C) Immunoblot analysis of chitobiase in liver extracts. Total lysates from liver of wild type and Ctbs deficient mice were resolved by SDS-PAGE and immunoblotted with anti-chitobiase antibody. β-actin was used as a loading control.

Out of 100 ES cell clones screened with PCR analysis, 5 indicated homologous recombination. Subsequent Southern blot analysis of EcoRI digested genomic DNA confirmed the disruption of the Ctbs gene for all of these clones. The 525-bp 5' flanking probe detected a 6.1 kb EcoRI fragment of the wild-type allele, and a 5.0 kb specific fragment of the targeted allele. Two targeted ES cell clones were chosen for injection into C57BL/6 blastocysts. Male chimeras with high contribution of agouti colour suggesting germ line transmission of the disrupted Ctbs allele were mated with wild type females. As expected, 50% of the F1 mice were heterozygous for the NEO insertion. In order to generate Ctbs−/− mice, heterozygous mice were crossed and the genotype of offspring was determined by Southern blot analysis (Fig. 1, panel C). For rapid genotyping of mice a PCR was designed in which the wild-type allele yielded a 2.7 kb fragment and the disrupted Ctbs allele a 3.2 kb fragment. (see Fig. 1, panel D).

Because Ctbs is abundantly expressed in kidney [14], total RNA was isolated from kidneys of wild-type (+/+), and homozygous Ctbs-deficient (−/−) mice. As expected, Ctbs mRNA was expressed in wild-type mice and absent in Ctbs-deficient mice (Fig. 1, panel E).

3.2. Enzyme activity

di-N-acetylchitobiose is commonly used as a substrate to quantify chitobiase activity. However, at least one other lysosomal enzyme, β-Hex, is able to hydrolyze this disaccharide [2]. This glycosidase can be distinguished from chitobiase due to its ability to hydrolyze the fluorimetric substrate 4-Methylumbelliferyl-N-acetyl-β-D-glucosaminide (MUG). Homozygous mutant mice were assayed and compared to wild-type animals at the age of 10 weeks. In tissues with high Ctbs expression levels, like liver and kidney [14], the measured activity towards chitobiose was reduced to roughly 50% in KO mice. The MUG activity, however, remained unaltered, suggesting that β-Hex was not the involved enzyme (Fig. 2, panel A). In tissues, like heart, where chitobiase is expressed at low levels, activity in KO mice was similar to that in WT ones. In order to separate chitobiase from β-Hex, a gel filtration was carried out, as described in Materials and Methods. Two β-Hex peaks were obtained, probably due to the two forms β-Hex B and β-Hex A with molecular masses of 130KDa and 120KDa respectively. Chitobiase, molecular weight 43 kDa [5], eluted after β-Hex, as expected. In KO tissues, the peak corresponding to chitobiase was completely absent, confirming the loss of chitobiase expression (Fig. 2, panel B).

Interestingly, the elution profile for chitobiase showed an additional peak lacking activity towards the synthetic substrate, indicating the presence of an additional enzyme able to hydrolyze the disaccharide at acidic pH with a molecular weight greater than that of β-Hex.

The β-Hex activity was assayed again at the age of 40 weeks, together with those of α-mannosidase and β-glucosidase. β-Hex activities were significantly increased in the mutant when compared with the wild-type tissues, whereas α-mannosidase showed a tendency for elevation (except brain) and the β-glucosidase activity was similar in KO and wild type mice (Fig. 3, panel A). Real-time PCR analysis showed increased expression levels of β-Hex and, to a minor extent, α-mannosidase in KO tissues, whereas β-glucosidase mRNA resulted unchanged (Fig. 3, panel B).

3.3. Immunoblotting

Western blot analysis using a polyclonal anti-chitobiase antibody, obtained as described in Materials and methods, revealed a signal corresponding to chitobiase in liver and kidney of normal mouse, while in deficient tissues no specific bands were detected, confirming that the expression of the protein was completely abolished. In Fig. 2 panel C a representative Western blot of liver is shown.

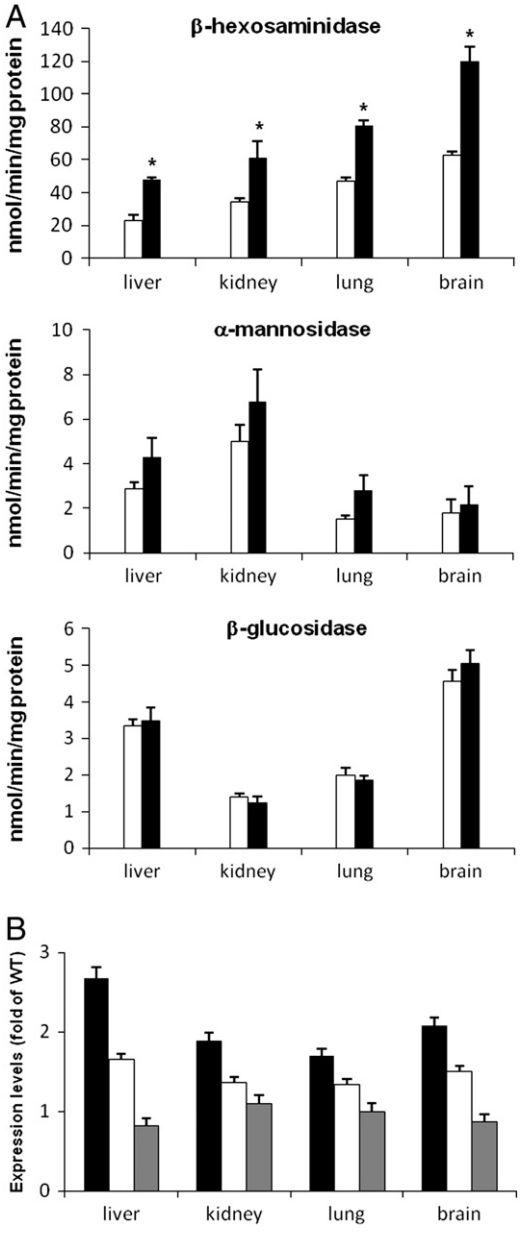

Fig. 3. β-hexosaminidase, α-mannosidase and β-glucosidase enzyme activity and gene expression assay. (A) Three wild type (white bars) and three homozygous mutant mice (black bars) were analyzed at the age of 40 weeks. Error bars represent one standard deviation. β-hexosaminidase activity increased in assayed tissues of knockout mice when compared with wild type. Asterisks indicate a significant difference ($P<0.05$). In liver, kidney and lung, but not brain, α-mannosidase showed a tendency for higher activity in KO mice compared to wild type control. β-glucosidase activity showed no difference between mutant and wild type mice. (B) β-hexosaminidase (black bars), α-mannosidase (white bars) and β-glucosidase (gray bars) expression fold changes in 40-week-old KO mouse tissues over WT control tissues. Two KO and two WT mice were used for the analysis, each assay was run in triplicate. The differences in expression levels are consistent with the activity profiles.

3.4. Pathological findings in organs

The most obvious changes in CTBS−/− mice were seen even in light microscopy in the kidney, where intensely stained storage material was found (Fig. 4) in a scattered subpopulation of epithelial cells exclusively of proximal tubules situated deep in the cortex. The extent and severity of storage was highly variable, ranging from minute dots barely visible in oil immersion up to conglomerates filling the major part of an epithelial cell. In a subfraction of tubules, entire epithelial cells as well as cellular debris were seen to fill the tubule

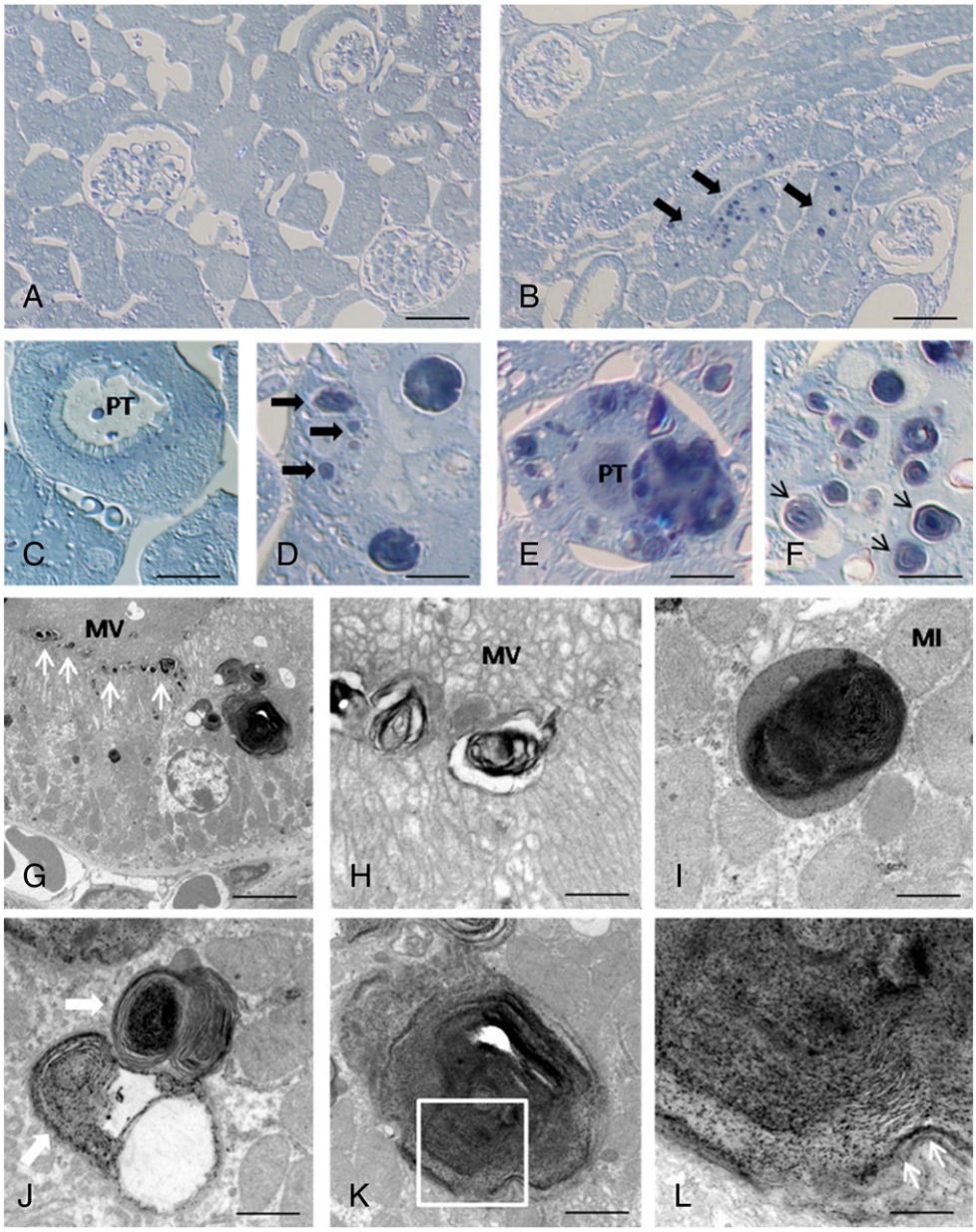

Fig. 4. Kidney involvement in Ctbs deficiency. (A, B) Low-power micrographs of WT (A) and KO (B) kidney indicate the presence of dark inclusion bodies (arrows in B) in a subset of proximal tubules. At higher magnification (WT shown in C, KO in D–E) it can be shown that this material can reside within epithelial cells themselves (arrows in D) at sometimes spectacular sizes (E) or even fill the tubule lumen, probably after disintegration of affected cells (PT in E). Even at medium magnification, a lamellar structure of the stored material can sometimes be discerned (arrows in F). Low-power electron microscopy clearly indicates that small inclusion bodies (white arrows in G) are lined up at the basis of the microvilli (MV), while larger accumulations of stored material typically reside deeper within the cells. Higher magnification reveals a multilamellar, onion shell-like substructure of already these smaller aggregates, apparently surrounded by a somewhat detached outer membrane. Medium-sized inclusion (diameter approx. 0.5 μm, I) may also be surrounded by a homogenous matrix within a membrane-bound compartment.. Larger inclusions (J–L; L representing an enlargement of the white box in K) are characterized by a densely packed multilamellar structure, often surrounding a strongly contrasting amorphous core, indicative of at least a major contribution of polar lipids to the stored material. Scale bars 300 μm in A and B, 30 μm in C and F, 15 μm in D and E; 7 μm in G, 50 nm in H, 300 nm in I–K, and 100 nm in L.

lumen. The stored material was selectively and intensely stainable with the lipid-selective dye p-phenylene diamine, pointing towards a significant amount of lipids enclosed here.

In TEM, it was striking that the intensely contrasted storage material was often organized in multilamellar myelin figures, again pointing towards a major content of (polar) lipids. Moreover, we often observed an intracellular gradient within the affected cells, with very small inclusion bodies lined up immediately below the actin network underlying the microvilli, and larger conglomerates deeper within the cell, which could be interpreted as an origin of stored material linked to the resorptive capacity of these cells.

After the initial observation of storage material developing in association with brush borders and thus with epithelia performing high-capacity resorption of material from a lumen, cells with a similar differentiation and function like intestinal epithelia were investigated in detail. However, epithelia of the proximal kidney tubule remained the sole cell type affected by this type of storage.

Lectin screening using chitobiase-binding lectins did not reveal differences between WT and KO kidney, only with lectins against mannosyl compounds a generalized staining of the apical half of proximal tubule epithelial cells was observed in KO and was absent in WT mice, which could indicate that the scattered storage seen in

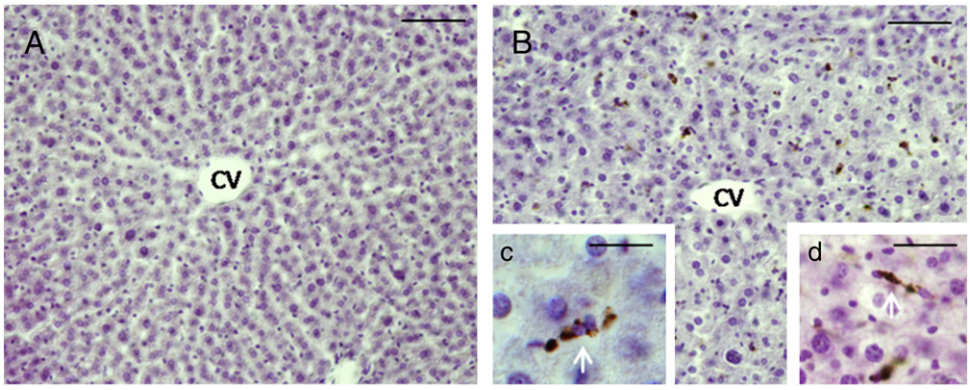

Fig. 5. Hematoxylin–eosoin-stained liver sections of WT (A) and Ctbs KO (B, c, d) mice showing central veins (CV) and surrounding liver lobules. Note the occurrence of multiple enlarged Kupffer cells filled with strongly pigmented phagocytosed material in KO tissue (shown in enlarged detail in c and d).

TEM might only represent those cells in which glycan accumulation has caused decompensation on the cell biological level (data not shown).

A less constant effect of CTBS deficiency was seen in liver, where a subpopulation of vesiculated Kupffer cells presented with increased size (Fig. 5).

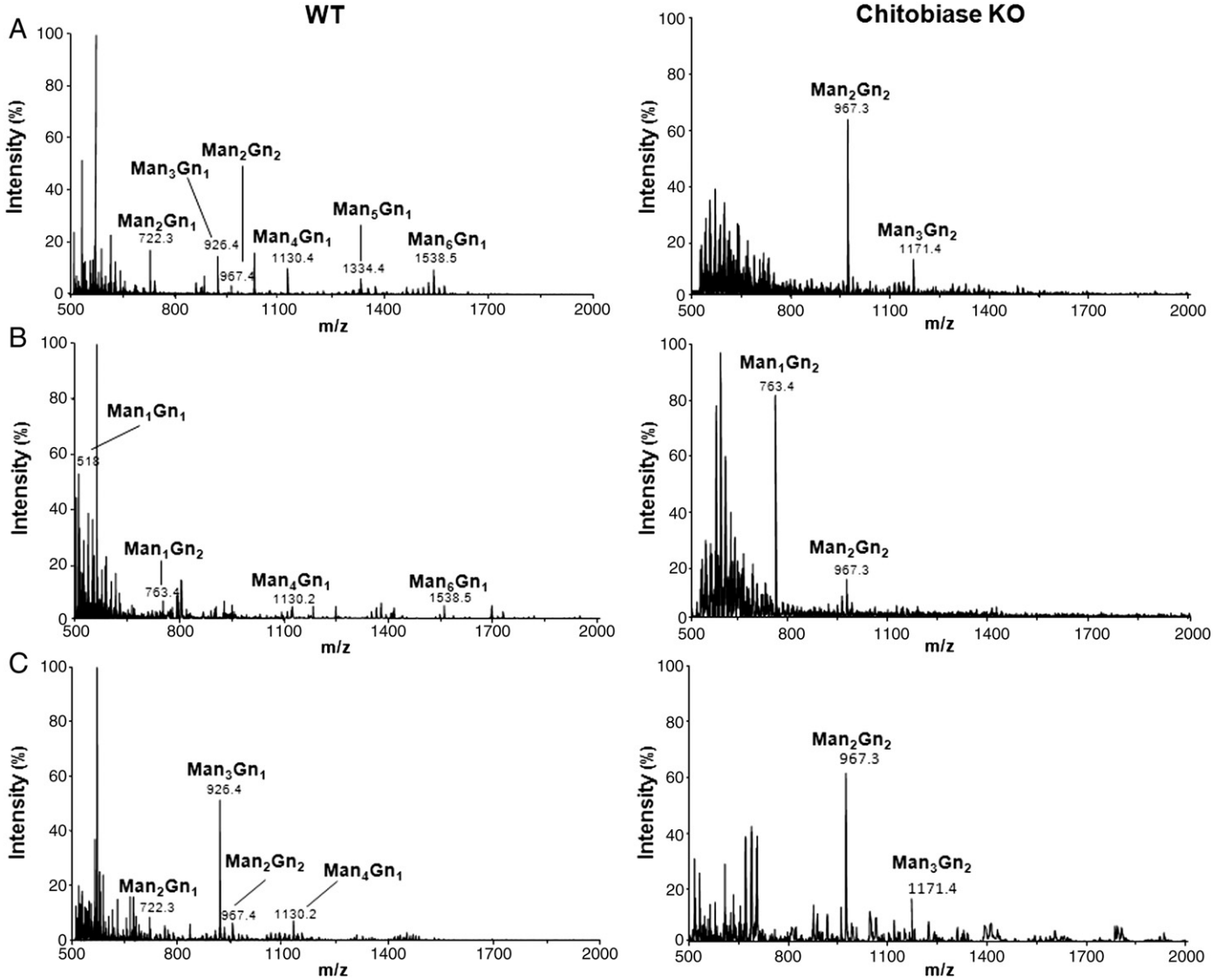

Fig. 6. MALDI TOF analysis of oligosaccharides after α-mannosidase treatments. Permethylated oligosaccharides extracted from wild type (WT) and chitobiase KO liver were analyzed by MALDI TOF after treatment with jack bean α-mannosidase or saitoi α-mannosidase. (A), control; (B), treatment with jack bean α-mannosidase; (C), treatment with *saitoi* α-mannosidase.

The lipid accumulation in kidneys from knockout mice was investigated by TLC analysis. However, no quantitative or qualitative differences between the lipid profiles of wild type and CTBS knockout tissues were evident (data not shown). However, this negative result could be due to sensitivity problems, as only a restricted number of proximal tubules is affected in each KO mouse.

3.5. Structural analyses of accumulated oligosaccharides in chitobiase KO mice tissues

To obtain functional evidence of the consequences of knockout chitobiase expression, structural analysis of free oligosaccharides was performed in liver and kidney of KO and WT mice. Free oligosaccharides were extracted from cellular homogenates and permethylated prior to analysis by MALDI-TOF MS. While in WT tissues a series of oligosaccharides representing Man2–6GlcNAc1, essentially originating from the endoplasmic reticulum-associated protein degradation (ERAD) process, were detected, in KO tissues two major oligosaccharides were observed (in Fig. 6 the spectrum obtained from liver is shown. Similar results have been obtained from kidney, data not shown). According to their *m/z* ratio, 967 and 1171, monosaccharide composition in terms of Hex and HexNAc have been determined as Hex2HexNAc2 and Hex3HexNAc2, respectively. Based on GC-MS data these oligosaccharides have been assigned to Man2-GlcNAc2 and Man3GlcNAc2, respectively.

Linkage analyses on Man2GlcNAc2 oligosaccharides were performed by GC-MS. Results expressed in Table 1 are fully consistent with the presence of a major Manα1–6Manβ1–4GlcNAcβ1–4GlcNAc oligosaccharide and, in lower concentration, of the tri-mannosyl core (Manα1–3[Manα1–6]Manβ1–4GlcNAcβ1–4GlcNAc) oligosaccharide.

To confirm the linkage results, oligosaccharides from WT and KO tissues were treated with jack bean α-mannosidase, able to hydrolyze α1–2, α1–3 and α1–6 linkages, or α-mannosidase from *Aspergillus saitoi*, specific for α1–2 linkage. After jack bean α-mannosidase treatment of KO samples, the molecular ion at *m/z* 1171 (Hex3HexNAc2) was abolished and the one corresponding to *m/z* 967 (Hex2HexNAc2) was significantly decreased with an increasing appearance of a signal consistent with the core of N-glycans Hex1HexNAc2 (*m/z* 763). In contrast, after treatment with α-mannosidase from *Aspergillus saitoi* molecular ions at *m/z* 1171 and 967 remained intact (Fig. 6). A major peak corresponding to Manβ1–4GlcNAc appears in WT jack bean α-mannosidase treated oligosaccharides, while the peak consistent with Man3GlcNAc1 species was predominant after α1–2 specific mannosidase treatment.

3.6. Quantitative analysis of accumulated Man2GlcNAc2 and Man3GlcNAc2

Quantification of accumulated oligosaccharides was performed by using a semi-quantitative experiment using the isotopic permethylation of an internal standard with $^{13}CH3I$ as previously described [20]. As observed in Fig. 7, Manα1–6Manβ1–4GlcNAcβ1–4GlcNAc oligosaccharide was significantly increased in all KO mouse tissues and particularly in liver. Even if the accumulation of the tri-mannosyl core (Manα1–3[Manα1–6]Manβ1–4GlcNAcβ1–4GlcNAc) oligosaccharide was less, its presence is observed in all tissues with a predominant appearance in lung and brain.

Table 1
GC Linkage analysis of partially methylated alditol acetates derivatives of Hex2HexNAc2 and Hex3HexNAc2 oligosaccharides accumulated in KO mice tissues.

Retention time (min)	Characteristic fragment ions	Assignment	Relative abundance
21.12	102, 118, 129, 145, 161, 162, 205	Terminal mannose	0.46
27.03[a]	102, 118, 129, 162, 189, 233	6-Linked mannose	0.46
36.21	117, 159, 233	4-Linked GlcNAc	1.00
31.24[b]	118, 129, 189, 234	3,6-Linked mannose	0.10

[a] Signals significantly decreased after treatment with jack bean α-mannosidase.
[b] Signals not observed after treatment with jack bean α-mannosidase.

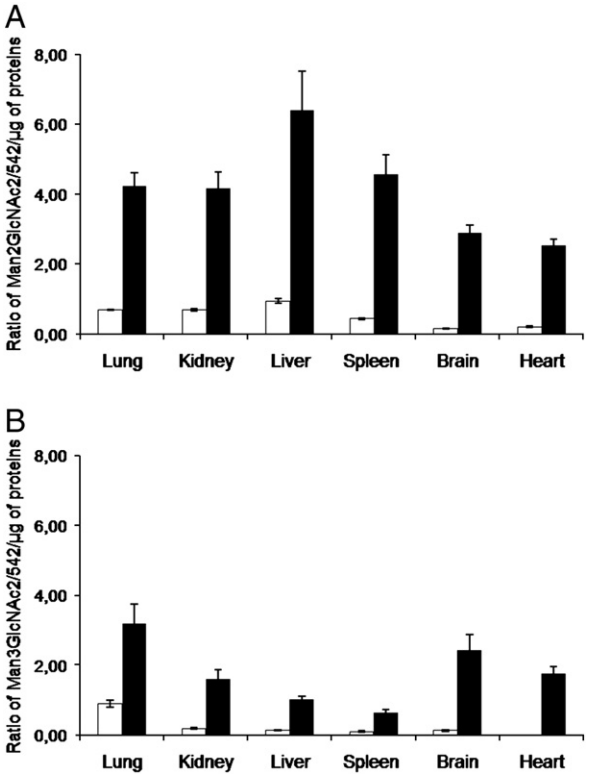

Fig. 7. Quantitative analysis of accumulated Man2GlcNAc2 (A) and Man3GlcNAc2 (B) in chitobiase KO mice tissues. After extraction from wild-type (white bars) and chitobiase KO (black bars) mouse tissues, soluble oligosaccharides were permethylated and mixed with a permethylated standard. Quantification of oligosaccharides was performed by calculating the ratio of peak height taking the oligosaccharide standard as reference. The values were normalized to the quantity of proteins in mg. For all assays, values are means ± SD of three independent experiments.

3.7. Analyses of oligosaccharides in urines

Urine of Ctbs KO mice was analyzed in order to detect the presence of the oligosaccharides accumulated in the tissues. Man2-GlcNAc2 concentration in KO urines is up to 10-fold higher than WT. The presence of Man3GlcNAc2 was observed at low levels in

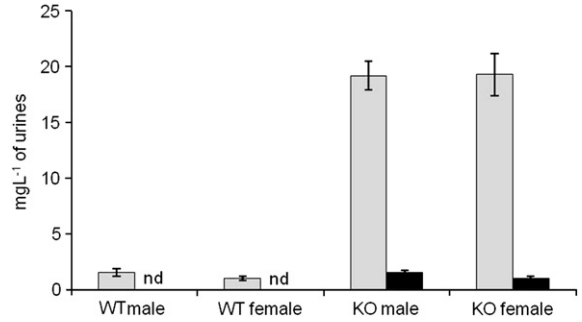

Fig. 8. Quantitative analysis of accumulated Man2GlcNAc2 (gray bars) and Man3-GlcNAc2 (black bars) in chitobiase KO mice urines. Soluble oligosaccharides were permethylated and mixed with a permethylated standard and were analyzed by MALDI TOF. Quantification of oligosaccharides was performed by calculating the ratio of peak height taking the known amount of oligosaccharide standard as reference. For all assays, values are means ± SD of three independent experiments. Man3GlcNAc2 species was not detected in wild type mice urines (nd: not detected).

KO urine, while it was not detected in urine of normal animals (Fig. 8).

4. Discussion

During the degradation of glycoproteins in lysosomes, the different glycosidic linkages in N-linked glycans are hydrolyzed by highly specific glycosidases, following a highly ordered pathway. Therefore a defect in a single enzyme will result in the accumulation of its substrate, causing a lysosomal storage disease [21]. A specific known storage disorder is associated to each of the enzyme participating at the N-linked glycan catabolism. The only exceptions are represented by chitobiase and core specific α1–6mannosidase, as corresponding lysosomal diseases have not been identified to date.

We have generated chitobiase KO mouse lines by gene targeting. A polyclonal anti-chitobiase rabbit antibody was used to demonstrate that immunoreactivity for chitobiase was absent in tissues of knockout mice. Gel filtration chromatography confirmed that there was no chitobiase activity in such tissues.

Chitobiase KO mice are fertile and have a normal appearance up to 1 year of age. Nevertheless, they present pathological features common to other animal models of lysosomal disorders: accumulation of oligosaccharides was present in all organs investigated which are liver, kidney, lung, spleen, heart and brain (staining with lectins specific for mannose residues confirmed the presence of mannose-containing oligosaccharides in all tested tissues) and the stored oligosaccharides are also excreted into urines at high levels; histological analysis revealed the presence of enlarged Kupffer cells in liver, already described in α-mannosidase- [22] and β-hexosaminidase B-deficient mice [23]; storage material accumulations in kidney proximal tubule epithelial cells resemble the membranous cytoplasmic bodies typical of G_{M2} gangliosidosis and are thus suggestive of polar lipids [24]. We could, however, not confirm lipid storage by biochemical methods.

While we could show accumulation of oligosaccharides in all tissues examined, we have evidence for the development of distinct storage material assemblies only for kidney and hepatic Kupffer cells. In kidney, surprisingly, only a small subset of proximal tubule epithelia develop the pathologic changes described above, pointing towards some still unexplained selectivity in cellular uptake, like specific receptors. Alternatively, storing cells could represent only early decompensating cells, which would be followed by a more systemic kidney damage at higher age. In any case, the situation seems to be strikingly different from glycolipid storage e.g. in Fabry disease, in which several renal cell types are affected in parallel.

Thus, if one assumes that the chitobiase KO mice resemble a so far unidentified human disease the possible human phenotype could be a purely renal disease. Alternatively, the accumulation of oligosaccharides without detectable storage material in other tissues could point to a late onset disease in which the accumulation has to proceed for some time before it manifests as microscopically visible storage material. This could result in a late onset disease with e.g. neurologic, renal and cardiac dysfunction.

The genetic lack of one lysosomal enzyme often leads to the increase of activities of the other enzymes in the same catabolic pathway, as happens in β-mannosidase knockout mice [25] and in caprine beta-mannosidosis [26]. We assayed β-hexosaminidase and α-mannosidase activity in 10 weeks and 40 weeks old chitobiase-deficient mice. At young age, there was no difference between normal and mutant tissues, whereas at older age β-hexosaminidase activity was statistically significantly increased in all tested tissues. Likewise α-mannosidase activity appeared higher in liver, kidney and lung from chitobiase-deficient mice than normal controls. β-glucosidase, an enzyme not involved in the N-linked glycoprotein degradation pathway, as expected had similar activity in mutant and wild type mice. The increase of β-hexosaminidase and α-mannosidase activity is due to a higher expression of the genes encoding for these hydrolases, suggesting the involvement of a cellular mechanism as a response to a stress condition. The enzymatic findings further indicate that the disruption of the Ctbs gene causes biochemical changes similar to other mouse models for lysosomal storage disorders.

Chitobiase and core specific α1–6mannosidase are differently expressed in tissues of various mammals. In ruminants, felines and dogs, expressing low levels of these enzymes, the classical α-mannosidase cleaves the α1–6 mannosidic linkage of the glycan core and the digestion of the chitobiose core is completed by the action of the β-hexosaminidase from the nonreducing end. In humans and rodents the trimming of α1–6 linked mannose of the glycan core is totally impaired if the chitobiose linkage is intact [7]. The N-acetylglucosamine at the reducing end is first removed by the chitobiase, and only subsequently the core specific α1–6 mannosidase cleaves the mannosidic linkage at the nonreducing end.

Therefore, the accumulation of Manα1–6Manβ1–4GlcNAcβ1–4-GlcNAc observed in chitobiase-KO mice is in accordance with previous studies. In contrast, the presence of stored Manα1–3[Manα1–6] Manβ1–4GlcNAcβ1–4GlcNAc, even if to a minor extent, is not easily explainable. In fact, α-mannosidase is known to cleave the α1–3 mannosidic linkage, regardless of the structure at the reducing end of the oligosaccharide. However, the similarity of chitobiase and α1–6 mannosidase expression pattern in humans and rodents suggests that human subjects lacking chitobiase activity should accumulate the same material observed in knockout mice, and consequently present similar pathological features.

Patients affected by beta-mannosidosis, a storage disorder caused by beta-mannosidase deficiency, show accumulation of the disaccharide Manβ1–4GlcNAc, and present a mild heterogeneous clinical expression [27]. Mental retardation, dysmorphology, developmental delay and hearing loss are the most common symptoms [28–30]. Ruminants affected by the same pathology accumulate the trisaccharide Manβ1–4GlcNAcβ1–4GlcNAc, due to chitobiase deficiency. Affected animals have a severe phenotype, with features that include inability to stand, facial dysmorphism, intention tremors, digital joint hyperextension [31] and most cases do not survive to the neonatal period. Although a strict correlation between the length of the stored product and the severity of the pathology has not been clearly demonstrated, an accumulation of a tetrasaccharide should lead to the onset of a more severe disorder as compared to the phenotype seen in beta-mannosidosis. This hypothesis is supported by the observation that aspartylglycosaminuria, characterized by the lysosomal accumulation of Manα1–6Manβ1–4GlcNAcβ1–4GlcNAc-Asn, even if this is not the only stored molecule, is a progressive and ultimately fatal disease [32].

Recent studies revealed a high prevalence of lysosomal storage disorders among symptomatically treated patients with unclear diagnosis. Fabry disease, an X-linked lysosomal disease caused by the deficiency of the glycohydrolase α-galactosidase A, is a striking example: a study on the frequency of unrecognised Fabry disease in a group of 721 patients suffering from acute cryptogenic stroke pointed out that the 4.9% of male patients and the 2.4% of women had a biologically significant mutation within the α-galactosidase A gene [33]. Similar screenings identified previously undiagnosed Fabry disease in 1%–4% of patients with hypertrophic cardiomyopathy [34,35] and in 0.36%–1.2% of males receiving hemodialysis [36,37].

4.1. Conclusions

The pathological features of chitobiase-deficient mice described in this work demonstrate *in vivo* that the complete breakdown of N-linked oligosaccharides in lysosomes requires the action of chitobiase, despite the presence of other enzymes able to hydrolyze the chitobiose core, like β-hexosaminidase. Moreover, the accumulation of

an unpredicted glycan structure (Man3GlcNAc2) opens new perspectives in studying the oligosaccharides degradating pathway.

The recent findings on the actual rate of lysosomal diseases in incompletely diagnosed patients under treatment, suggest that a genetic defect of the chitobiase should be the cause of a not yet described lysosomal storage disease and affected patients could be already in therapy without a complete diagnosis. The in-depth characterization of the chitobiase knockout mouse model will provide a precise panel of symptoms for the identification of such patients. Preliminary data from the mouse model may indicate that this putative disease would be milder and/or clinically present at higher ages than gangliosidoses and may not have major neurological symptoms. A genomic screening for mutations/deletions in the chitobiase gene on subjects with comparable symptoms and an incomplete diagnosis could identify chitobiase-deficient patients.

Acknowledgements

The authors thank Marcello Coli for his precious contribution for the production of the anti-chitobiase antibody, Dr. Catherine Robbe-Masselot, Angelika Zoons and Birgit Rau for their technical support.

This work was financially supported by Vaincre les Maladies Lysosomales, Massy, France.

References

[1] N.N. Aronson Jr., M. Kuranda, Lysosomal degradation of Asn-linked glycoproteins, FASEB J. 3 (1989) 2615–2622.
[2] J.L. Stirling, FEBS Lett. 39 (1974) 171–175.
[3] K.J. Fisher, N.N. Aronson Jr., Cloning and expression of the cDNA sequence encoding the lysosomal glycosidase Di-N-acetylchitobiase, J. Biol. Chem. 267 (1992) 19607–19616.
[4] P.F. Daniel, J.E. Evans, R. De Gasperi, B. Winchester, C.D. Warren, A human lysosomal alpha(1–6)-mannosidase active on the branched trimannosyl core of complex glycans, Glycobiology 2 (1992) 327–336.
[5] J.F. Haeuw, T. Grard, C. Alonso, G. Strecker, J.C. Michalski, The core-specific lysosomal alpha(1–6)-mannosidase activity depends on aspartamidohydrolase activity, Biochem. J. 297 (1994) 463–466.
[6] B. Winchester, Lysosomal metabolism of glycoproteins, Glycobiology 15 (2005) R1–R15.
[7] C. Park, L. Meng, L.H. Stanton, R.E. Collins, S.W. Mast, X. Yi, H. Strachan, K.W. Moremen, Characterization of a human core-specific lysosomal α1,6-mannosidase involved in N-glycan catabolism, J. Biol. Chem. 280 (2005) 37204–37216.
[8] E. Kelo, U. Dunder, I. Mononen, Massive accumulation of Man2GlcNAc2–Asn in nonneuronal tissues of glicosylasparaginase-deficient mice and its removal by enzyme replacement therapy, Glycobiology 15 (2005) 79–85.
[9] N.N. Aronson, M. Backes, M.J. Kuranda, Rat liver chitobiase: purification, properties, and role in the lysosomal degradation of Asn-linked glycoproteins, Arch. Biochem. Biophys. 272 (1989) 290–300.
[10] B. Liu, W. Ahmad, N.N. Aronson Jr., Structure of the human gene for lysosomal di-N-acetylchitobiase, Glycobiology 9 (1999) 589–593.
[11] D. Abraham, W.F. Blakemore, R.D. Jolly, R. Sidebotham, B. Winchester, The catabolism of mammalian glycoproteins. Comparison of the storage products in bovine, feline and human mannosidase, Biochem. J. 215 (1983) 573–579.
[12] K. Yamashita, Y. Tachibana, K. Mihara, S. Okada, H. Yabuuchi, A. Kobata, Urinary oligosaccharides of mannosidosis, J. Biol. Chem. 255 (1980) 5126–5133.
[13] P.F. Daniel, B. Winchester, C.D. Warren, Mammalian alpha-mannosidases multiple forms but a common purpose, Glycobiology 4 (1994) 551–566.
[14] C. Balducci, L. Bibi, T. Berg, E. Persichetti, R. Tiribuzi, S. Martino, S. Paciotti, R. Roberti, A. Orlacchio, T. Beccari, Molecular cloning and structural organization of the gene encoding the mouse lysosomal di-N-acetylchitobiase (ctbs), Gene 416 (2008) 85–91.
[15] T.M. Magin, J. McWhir, D.W. Melton, A new mouse embryonic stem cell line with good germ line contribution and gene targeting frequency, Nucleic Acids Res. 20 (1992) 3795–3796.
[16] U. Matzner, E. Herbst, K.K. Hedayati, R. Lüllmann-Rauch, C. Wessig, S. Schröder, C. Eistrup, C. Möller, J. Fogh, V. Gieselmann, Enzyme replacement improves nervous system pathology and function in a mouse model for metachromatic leukodystrophy, Hum. Mol. Genet. 14 (2005) 1139–1152.
[17] J.K. Yao, G.M. Rastetter, Microanalysis of complex tissue lipids by high-performance thin-layer chromatography, Anal. Biochem. 150 (1985) 111–116.
[18] D. Kmiécik, V. Herman, C.J. Stroop, J.C. Michalski, A.M. Mir, O. Labiau, A. Verbert, R. Cacan, Catabolism of glycan moieties of lipid intermediates leads to a single Man5GlcNAc oligosaccharide isomer: a study with permeabilized CHO cells, Glycobiology 5 (1995) 483–494.
[19] W. Morelle, V. Faid, F. Chirat, J.C. Michalski, Analysis of N- and O-linked glycans from glycoproteins using maldi-tof mass spectrometry, Methods Mol. Biol. 534 (2009) 1–19.
[20] G. Alvarez-Manilla, N.L. Warren, T. Abney, J. Atwood, P. Azadi, W.S. York, M. Pierce, R. Orlando, Tools for glycomics: relative quantitation of glycans by isotopic permethylation using 13CH3I, Glycobiology 17 (2007) 677–687.
[21] B.G. Winchester, Lysosomal metabolism of glycoconjugates, Subcell. Biochem. 27 (1996) 191–238.
[22] S. Stinchi, R. Lüllmann-Rauch, D. Hartmann, R. Coenen, T. Beccari, A. Orlacchio, K. von Figura, P. Saftig, Targeted disruption of the lysosomal alpha-mannosidase gene results in mice resembling a mild form of human alpha-mannosidosis, Hum. Mol. Genet. 8 (1999) 1365–1372.
[23] D. Phaneuf, N. Wakamatsu, J.Q. Huang, A. Borowski, A.C. Peterson, S.R. Fortunato, G. Ritter, S.A. Igdoura, C.R. Morales, G. Benoit, B.R. Akerman, D. Leclerc, N. Hanai, J.D. Marth, J.M. Trasler, R.A. Gravel, Dramatically different phenotypes in mouse models of human Tay–Sachs and Sandhoff diseases, Hum. Mol. Genet. 5 (1996) 1–14.
[24] R.A. Gravel, J.T.R. Clarke, M.M. Kaback, D. Mahuran, K. Sandhoff, K. Suzuki, The GM2 gangliosidoses, in: C.R. Scriver, A.L. Beaudet, W.S. Sly, D. Valle (Eds.), The Metabolic and Molecular Bases of Inherited Disease, McGraw–Hill, New York, 1995, pp. 2839–2879.
[25] M. Zhu, K.L. Lovell, J.S. Patterson, T.L. Saunders, E.D. Hughes, K.H. Friderici, Beta-mannosidosis mice: a model for the human lysosomal storage disease, Hum. Mol. Genet. 15 (2006) 493–500.
[26] K.L. Lovell, R.J. Kranich, K.T. Cavanagh, Biochemical and histochemical analysis of lysosomal enzyme activities in caprine beta-mannosidosis, Mol. Chem. Neuropathol. 21 (1994) 61–74.
[27] A. Cooper, C.E. Hatton, M. Thornley, I.B. Sardharwalla, Alpha- and beta-mannosidosis, J. Inherit. Metab. Dis. 13 (1990) 538–548.
[28] H.M. Riise Stensland, E. Persichetti, C. Sorriso, G.M. Hansen, L. Bibi, S. Paciotti, C. Balducci, T. Beccari, Identification of two novel beta-mannosidosis-associated sequence variants: biochemical analysis of beta-mannosidase (MANBA) missense mutations, Mol. Genet. Metab. 94 (2008) 476–480.
[29] F. Sabourdy, P. Labauge, H.M. Stensland, M. Nieto, V.L. Garcés, D. Renard, G. Castelnovo, N. de Champfleur, T. Levade, A MANBA mutation resulting in residual beta-mannosidase activity associated with severe leukoencephalopathy: a possible pseudodeficiency variant, BMC Med. Genet. 10 (2009) 84.
[30] P. Labauge, D. Renard, G. Castelnovo, F. Sabourdy, N. de Champfleur, T. Levade, Beta-mannosidosis: a new cause of spinocerebellar ataxia, Clin. Neurol. Neurosurg. 111 (2009) 109–110.
[31] B. Abbitt, M.Z. Jones, T.R. Kasari, R.W. Storts, J.W. Templeton, P.S. Holland, P.E. Castenson, Beta-mannosidosis in twelve Salers calves, J. Am. Vet. Med. Assoc. 198 (1991) 109–113.
[32] P. Arvio, M. Arvio, Progressive nature of aspartylglucosaminuria, Acta Paediatr. 91 (2002) 255–257.
[33] A. Rolfs, T. Bottcher, M. Zshiesche, P. Morris, B. Winchester, P. Bauer, U. Walter, E. Mix, M. Lohr, K. Harzer, U. Strauss, J. Pahnke, A. Grossmann, R. Benecke, Prevalence of Fabry disease in patients with cryptogenic stroke: a prospective study, Lancet 366 (2005) 1794–1796.
[34] L. Monserrat, J.R. Gimeno-Blanes, F. Marín, M. Hermida-Prieto, A. García-Honrubia, I. Pérez, X. Fernández, R. de Nicolas, G. de la Morena, E. Payá, J. Yagüe, J. Egido, Prevalence of Fabry disease in a cohort of 508 unrelated patients with hypertrophic cardiomyopathy, J. Am. Coll. Cardiol. 50 (2007) 2399–2403.
[35] B. Sachdev, T. Takenaka, H. Teraguchi, C. Tei, P. Lee, W.J. McKenna, P.M. Elliott, Prevalence of Anderson–Fabry disease in male patients with late onset hypertrophic cardiomyopathy, Circulation 105 (2002) 1407–1411.
[36] D.B. Porsch, A.C. Nunes, V. Milani, L.B. Rossato, C.B. Mattos, M. Tsao, C. Netto, M. Burin, F. Pereira, U. Matte, R. Giugliani, E.J. Barros, Fabry disease in hemodialysis patients in southern Brazil: prevalence study and clinical report, Ren. Fail. 30 (2008) 825–830.
[37] S. Nakao, C. Kodama, T. Takenaka, A. Tanaka, Y. Yasumoto, A. Yoshida, T. Kanzaki, A.L.D. Enriquez, C.E. Eng, H. Tanaka, C. Tei, R.J. Desnick, Kidney Int. 64 (2003) 801–807.